Binding weakly interacting partners: A study of Ca–He_2 and its isotopomers

David López-Durán, Rocío Rodríguez-Cantano, Tomás González-Lezana, Gerardo Delgado-Barrio, and Pablo Villarreal*
Instituto de Física Fundamental, IFF-CSIC, Serrano 123, 28006 Madrid, Spain

Franco A. Gianturco
Department of Chemistry and CNISM, University of Rome La Sapienza, Piazzale A. Moro 5, 00185 Rome, Italy
(Dated: May 2, 2012)

We present in this paper binding energies and structures of non-rotating weakly bound ^{40}Ca-^{n}He$_2$ triatomic complexes. Two kind of systems are discussed: bosonic ($n = 4$) and fermionic ($n = 3$) complexes at its singlet state (nuclear spin $S = 0$). Three different coordinate systems and methods have been used to solve the relevant Schrödinger equation: Variational calculations 1) using satellite coordinates and a discrete variable representation of radial functions, 2) employing pair coordinates and products of distributed Gaussian functions as basis functions, and 3) Variational/Diffusion Monte Carlo calculations in Cartesian coordinates. The potential energy surface is represented as the addition of pair potentials. By using the most realistic interaction between each pair of particles, present results from the three methods are in fair agreement. Only two bound states for each system are found in our computations.

PACS numbers: 31.15.ac, 33.15.Bh, 33.15.Fm

I. INTRODUCTION

Helium nanodroplets have received considerable attention in recent years because of their very special properties since a superfluid droplet made of ^{4}He atoms can provide an ideal matrix for spectroscopic studied around 300-400 mK[1, 2]. The superfluidity of such nanodroplets is in fact instrumental in allowing even rotationally resolved spectra of molecules solvated in ^{4}He environment[3]: for the case of atoms, for instance, the shifts of the electronic transition lines represent a very useful observable to determine the location of that foreign atom attached to a specific ^{3,4}He droplet since, while most impurities (atomic and molecular) are found to reside in the interior of the droplets[4], it is also well established that, because of their weak interactions, alkali atoms preferentially reside in a "dimple" at the surface of the drops for both helium isotopes[5, 6]. The question of establishing solvation instead of surface location for an impurity atom in a helium droplet is therefore of great importance to further understand the behavior of the spectroscopic observations as a function of the droplet' s size for a given alkali atom [7]. In particular in the case of the Ca atoms it becomes important to be able to select the most realistic interaction between the electronic ground state of the latter and the ^{3,4}He droplet under consideration in order to then compare the strength of that potential with the one describing the He-He forces within the droplet[8].

The needed interaction between Ca and He atoms has been studied and proposed by various publications in recent years. The modeling of it via simple empirical formulae was put forward by Kleinekathöfer in the year 2000[9], where he found a minimum well depth of about 15 K at a distance of 9.64 a_0. Earlier calculations of Stinkenmeier et al.[10] had provided a well depth of about 20 K at a minimum distance of 10.3 a_0. On the other hand, *ab initio*, quantum chemical calculations which came out after the above work suggested a very different scenario: The work of Lovallo and Klobukowski[11] using Coupled Clusters with single, double and (perturbation) triple excitations (CCSD(T)) found an equilibrium distance of about 11 a_0 and a well depth of about 5 K, in line with CASSCF calculations carried out by Czuchaj et al.[12] that reported an r_{eq} of 11.05 a_0 and a well depth of about 6 K. Partridge et al.[13] also indicated an r_{eq} of 11.2 a_0 and a well depth of about 5 K. Very accurate quantum chemical studies of R. J. Hinde[14] of the Ca He complex indeed produced a well depth of about 5 K once more and an equilibrium distance of about 9 a_0.

Thus, we can say that the recently proposed Ca–He potential energy curves (PECs) fall into two different groups and , although both place the equilibrium distance in the region of about 10 a_0, one set of estimates[9, 10] indicate a well depth of about 16 K or more, while another group of *ab initio* studies[11–14] indicates that same well to have a much shallower depth of about 5 K. A very recent computational study on the binding of the three partners[15]

*Corresponding author: p.villarreal@iff.csic.es

has employed the same potential form indicated by Eq. (1) and used the He–He PEC from Ref.[16] together with the stronger Ca–He PEC of Ref.[9]. Here we present detailed calculations employing the form suggested by quantum chemical *ab initio* studies, in particular that of Ref.[11].

In the present study we therefore intend to look in some detail at the features and strength of binding a calcium atom with at most two He atoms, to model with them the simplest description of an helium aggregate attached to that impurity. Choosing initially this three–particle complex will be able to help us in producing very accurate and realistic descriptions of the forces at play, as well as giving us some indication on the likely evolution of the binding strength for larger aggregates. The paper is organized as follows: The next section briefly describes the intermolecular forces selected in the present study, while section III will provide details on our computational methods. Section IV will present and discuss the results we have obtained on Ca^4He_2 and Ca^3He_2 complexes, while Section V will summarize our conclusions.

II. THE INTERACTION POTENTIALS

The weakness of the interaction between the partners of the present complex allows one to represent the potential energy surface (PES) as a simple sum of two–body (2B) potentials

$$V(R_1, R_2, R_3) = \sum_{k=1}^{2} V_{\mathrm{Ca-He}}(R_k) + V_{\mathrm{He-He}}(R_3), \tag{1}$$

where R_1, R_2 are the two Ca-He distances and R_3 is the He-He distance. Therefore the next step in the implementation is to select realistic descriptions of the relevant 2B PECs. For the He-He interaction potential we have selected the one suggested earlier by Aziz and Slaman[16], which takes advantage of several features of the experimental data in order to parameterize a final PEC which has been employed several times already in our previous studies of similar clusters[17].

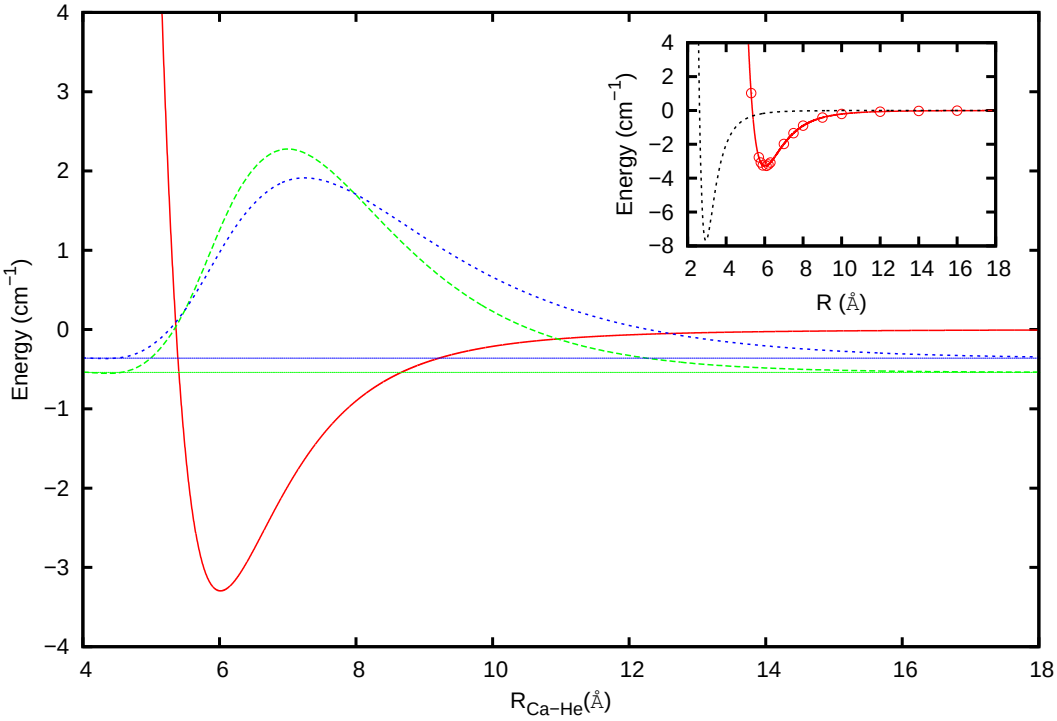

FIG. 1: Ca-He interaction up to 4 cm^{-1} analytically fitted to the points provided by Ref.[11], and pair distribution functions for the two helium isotopes, see text for further details. The dashed line refers to the bosonic dimer while the dots are for the fermionic case. The inset shows both He-He[16] and Ca-He interactions, where the raw points of Ref.[11] are also included.

The He-He [16] potential is analytical. We have also generated an analytical expression to describe the Ca-He interaction of Ref.[11]. To this end, for distances $r \geq 4.6$ Å, the raw points reported in Table VII of Ref.[11],and excluding the point at 6.0 Å which was found to be somewhat out of range with respect to the others, have been least-square fitted to an expansion in inverse even powers of r, while a Born-Mayer extrapolation of the curve has been done towards shorter distances ($r \leq 4.6$ Å)

$$\begin{aligned} V_{\mathrm{Ca-He}}(r) &= Ae^{-kr}/r \qquad r \leq 4.6 \quad \text{Å} \\ &= \sum_{n=3}^{7} c_{2n}/r^{2n} \qquad r \geq 4.6 \quad \text{Å}. \end{aligned} \tag{2}$$

The obtained values (distance in Å, energy in cm^{-1}) of the parameters are: $c_6 = -231619.170$, $c_8 = 15438995.509$, $c_{10} = -2085441484.937$, $c_{12} = 82383199752.866$, $c_{14} = -852545635932.049$, $A = 2040362.862$, and $k = 2.088$. The fitted curve presents an equilibrium distance of $r = 6.02$ Å and a well-depth of -3.2956 cm^{-1}. For energies below 5 cm^{-1}, which are relevant to the present study, the standard deviation of the fit with respect to the raw points[11] is only of 0.002 cm^{-1}. In Fig. 1 we display the analytical Ca-He interaction together with the distribution corresponding to the only vibrational bound state obtained for each isotopic variant of He. The high quality of the fit is clearly shown in the inset of Fig. 1, where the He-He interaction is also depicted for comparison. As can be realized, the latter presents its equilibrium distance around 3 Å, (two times shorter than the former) and a well-depth of ~ 7.7 cm^{-1} (more than twice the Ca-He interaction). Within a classical picture this situation suggests a closer packing of the helium atoms that pushes outside the calcium partner.

III. THEORETICAL METHODS

A. Discrete variable representation in satellite coordinates

After separation of the center of mass motion, the Hamiltonian describing the Ca–He_2 triatomic system can be written in satellite coordinates $\{\boldsymbol{R}_k\}$ as[18]

$$H = \sum_{k=1}^{2} \left[-\frac{\hbar^2}{2\mu}\frac{\partial^2}{\partial R_k^2} + \frac{\boldsymbol{l}_k^2}{2\mu R_k^2} + V_{\mathrm{Ca-He}}(R_k) \right] + \tilde{V}_{\mathrm{He-He}}, \tag{3}$$

where $\boldsymbol{R}_k$ are the vectors from the Ca atom to the different He atoms, $\boldsymbol{l}_k$ are the angular momenta associated with $\boldsymbol{R}_k$, μ is the reduced mass of the Ca–He system, and $V_{\mathrm{Ca-He}}$ represents the Ca–He interatomic potential. In Eq. (3) the He–He interaction $\tilde{V}_{\mathrm{He-He}}$ includes the potential $V_{\mathrm{He-He}}(R_3)$, which is readily expressed in terms of the internal coordinates R_1, R_2, and $\cos\gamma = \boldsymbol{R}_1 \cdot \boldsymbol{R}_2/R_1R_2$ through the cosine theorem, and a kinetic cross term arising from the use of non-Jacobi coordinates,

$$\tilde{V}_{\mathrm{He-He}} = V_{\mathrm{He-He}}(R_1, R_2, cos\gamma) - \frac{\hbar^2}{m_{\mathrm{Ca}}} \boldsymbol{\nabla}_{\boldsymbol{R}_1} \cdot \boldsymbol{\nabla}_{\boldsymbol{R}_2}. \tag{4}$$

In a space-fixed coordinate system, we consider the following basis functions:

$$\Phi^L_{q_1 q_2}(\boldsymbol{R}_1, \boldsymbol{R}_2) = f_{m_1}(R_1) f_{m_2}(R_2) \mathcal{Y}^L_{\ell_1 \ell_2}(\hat{\boldsymbol{R}}_1, \hat{\boldsymbol{R}}_2), \tag{5}$$

where f_{m_i} are radial functions associated with the Ca-He vibrations which will be further specified, and $\mathcal{Y}^L_{\ell_1\ell_2}$ are angular functions in the coupled representation,

$$\mathcal{Y}^L_{\ell_1\ell_2}(\hat{\boldsymbol{R}}_1, \hat{\boldsymbol{R}}_2) = (-1)^L \sqrt{2L+1} \sum_{\omega} \begin{pmatrix} \ell_1 & \ell_2 & L \\ -\omega & \omega & 0 \end{pmatrix} Y_{\ell_1\omega}(\theta_1, \phi_1) Y_{\ell_2 -\omega}(\theta_2, \phi_2), \tag{6}$$

where $\hat{\boldsymbol{R}}_k = \boldsymbol{R}_k/R_k = (\theta_k, \phi_k)$ are unit vectors, $\begin{pmatrix} \cdot & \cdot & \cdot \\ \cdot & \cdot & \cdot \end{pmatrix}$ are $3-j$ symbols, and $Y_{\ell_k\omega}$ are spherical harmonics. Here, L is the quantum number associated with the total angular momentum $\boldsymbol{L} = \boldsymbol{l}_1 + \boldsymbol{l}_2$, and ℓ_k and m_k (k=1, 2) are quantum numbers associated with the angular momenta $\boldsymbol{l}_k$ and the vibrations, respectively. They are collected into a set of quantum numbers $\{q_k\} = \{m_k \ell_k\}$.

The symmetry operations of the system are the total inversion $\mathcal{E}^*$, and the permutation of the He atoms $\mathcal{P}$. The functions of Eq. (5) are already eigenfunctions of $\mathcal{E}^*$,

$$\mathcal{E}^* \left[\Phi^L_{q_1 q_2}\right] = (-1)^{\ell_1+\ell_2}\Phi^L_{q_1 q_2}, \tag{7}$$

while the action of the permutation operator is

$$\mathcal{P} \left[\Phi^L_{q_1 q_2}\right] = (-1)^{\ell_1+\ell_2+L}\Phi^L_{q_2 q_1}. \tag{8}$$

Hence, one builds up a symmetry-adapted basis set of functions:

$$\Psi^{L\varepsilon\kappa}_{q_1 q_2} = \left[2(1+\delta_{m_1 m_2}\delta_{\ell_1 \ell_2})\right]^{-1/2} \left[\Phi^L_{q_1 q_2} + \varepsilon\kappa(-1)^L \Phi^L_{q_2 q_1}\right], \tag{9}$$

which are eigenfunctions of $\mathcal{E}^*$ and $\mathcal{P}$ with eigenvalues $\varepsilon = (-1)^{\ell_1+\ell_2}$ and κ, respectively. The Hamiltonian of Eq. (3) is readily represented in this basis. In particular, matrix elements of both terms in $\tilde{V}_{\mathrm{He-He}}$ of Eq. (4), as well as expressions for probability distributions of the variables R ($R = R_1$ or R_2), cosγ, or R_3, can be found in Ref. [19].

In turn, the vibrational basis set of functions $f_m(R)$ chosen are the fixed-node ones of Muckerman[20] leading to a discrete variable representation (DVR). They come from particle-in-a-box sine functions and are based on an equally weighted Gauss-Chebyshev quadrature of the second kind. Within an interval $[R_{in}, R_{fin}]$ of length $R_L = R_{fin} - R_{in}$, one chooses the equally spaced N points $R_m = R_{in} + mR_L/(N+1)$, $m = 1, N$. The corresponding orthogonal functions,

$$f_m(R) = 2\left[(N+1)R_L\right]^{-1/2} \sum_{k=1}^{N} sin\frac{km\pi}{N+1}\ sin\frac{k\pi(R-R_{in})}{R_L}, \tag{10}$$

fulfill the standard DVR property

$$\langle f_m\,|V(R)|f_{m'}\rangle = V(R_m)\,\delta_{mm'}, \tag{11}$$

while matrix elements of first and second derivatives become

$$\langle f_m\,|\frac{\mathrm{d}}{\mathrm{d}\,R}|f_{m'}\rangle = \frac{4}{(N+1)R_L} \sum_{k,k'=1}^{N} \frac{kk'}{k^2-k'^2}(1 - cos\,k\pi\ cos\,k'\pi) sin\frac{mk\pi}{N+1}\ sin\frac{m'k'\pi}{N+1}, \tag{12}$$

and

$$\langle f_m\,|\frac{\mathrm{d}^2}{\mathrm{d}\,R^2}|f_{m'}\rangle = -\frac{2\pi^2}{(N+1)R_L^2} \sum_{k=1}^{N} k^2 sin\frac{mk\pi}{N+1}\ sin\frac{m'k\pi}{N+1}, \tag{13}$$

respectively.

B. Distributed Gaussian functions method

The distributed Gaussian functions (DGF) method [21–23] has been employed before for different systems with two identical rare-gas atoms and an impurity atom as in the $LiHe_2$ [17], He_2H^- [24] and Ne_2H^- [25] complexes. The total Hamiltonian in this approach (for a zero total angular momentum) can be expressed via atom-atom coordinates as

$$H(R_1, R_2, R_3) = T + V(R_1, R_2, R_3), \tag{14}$$

where T is the kinetic operator and the potential V is expressed as the addition of pair interactions, see Eq. (1), in terms of R_1, R_2 (the two Ca-He distances) and R_3 (the He–He distance). The total wave function which ensures the standard normalization condition [25]:

$$\int\int\int dR_1 dR_2 dR_3 \mid \Phi \mid^2 = 1, \tag{15}$$

is eigenstate of the following Hamiltonian:

$$H(R_1,R_2,R_3) \;=\; \frac{-\hbar^2}{2\mu_{\rm Ca-He}}T_1+\frac{-\hbar^2}{m_{\rm Ca}}T_2+\sum_{i=1}^{2}V_{\rm HeCa}(R_i)+V_{\rm HeHe}(R_3). \tag{16}$$

The corresponding expressions for the T_1 and T_2 kinetic operators in terms of the interparticle coordinates are given explicitly in Ref. [17].

Within the DGF framework, the total wave function is expanded as follows:

$$\Phi_{\rm k}(R_1,R_2,R_3)=\sum_j a_j^{\rm (k)}\phi_j(R_1,R_2,R_3), \tag{17}$$

where

$$\phi_j(R_1,R_2,R_3)=N_{lmn}^{-1/2}\sum_{P\in S_2}P[\varphi_l(R_1)\varphi_m(R_2)]\varphi_n(R_3), \tag{18}$$

and the basis is symmetrized by means of the proper P permutation operator for the R_1 and R_2 coordinates. Here, j denotes a collective index such as j=($l\leq m;n$).

The corresponding normalization constants, N_{lmn}, are

$$N_{lmn}=2s_{nn}(s_{ll}s_{mm}+s_{lm}^2), \tag{19}$$

expressed in terms of the overlap integrals

$$s_{pq}=\langle\varphi_p|\varphi_q\rangle. \tag{20}$$

The φ_p functions are chosen to be DGFs centered at the R_p position [26]:

$$\varphi_p(R)=\sqrt[4]{\frac{2A_p}{\pi}}e^{-A_p(R-R_p)^2}. \tag{21}$$

where the coefficient $\rm A_p$ is defined in terms of the the centers of φ_{p-1} and φ_{p+1} as follows:

$$A_p=\frac{4\beta}{(R_{p+1}-R_{p-1})^2}. \tag{22}$$

For the specific cases of the first and the last DGFs we have the values $A_1=\beta/(R_{p=2}-R_{p=1})^2$ and $A_{N_{\rm last}}=\beta/(R_{p=N_{\rm last}}-R_{p=N_{\rm last}-1})^2$, respectively. In all the previous expressions β is a dimensionless parameter taken to be close to one. The product of DGFs $\varphi_l\varphi_m\varphi_n$ is included in the basis set if the corresponding centers verify the triangle requirement

$$\mid R_l-R_m\mid<R_n<R_l+R_m. \tag{23}$$

The non-orthogonal character of the chosen basis sets requires solving the generalized matrix eigenproblem:

$$\mathcal{H}\Phi=\mathcal{S}\Phi\mathcal{E}, \tag{24}$$

where $\mathcal{H}$ and $\mathcal{S}$ are the Hamiltonian and the overlap matrix, respectively, for the $\{\phi_j\}$ basis set.

C. Quantum Monte Carlo Methods

The quantum stochastic simulation employed in this work has been previously explained (see Refs. [27–29], for instance) and we present here only a brief outline. It is formed by a pure Variational Monte Carlo (VMC) calculation followed by a Diffusion Monte Carlo (DMC) approach. In the VMC step the energy is optimized with respect to the parameters of the trial wavefunction $\Psi_T(\mathbf{R})$, which in the case of a system formed by an impurity and N helium atoms can be expressed as the product of purely nodeless exponential forms [28]:

$$\Psi_T(\mathbf{R})=\Psi_{\rm Ca-He}(\mathbf{R})\Psi_{\rm He-He}(\mathbf{R}). \tag{25}$$

$\mathbf{R} \equiv \{\boldsymbol{R}_i\}_{i=1}^{N}$ is the collective index that bring together the coordinates $\boldsymbol{R}_i$ of the rare gas particles, while $\Psi_{\mathrm{Ca-He}}(\mathbf{R})$ and $\Psi_{\mathrm{He-He}}(\mathbf{R})$ are the Ca-He and the He-He part of the wavefunction, respectively:

$$\Psi_{\mathrm{Ca-He}}(\mathbf{R}) = \prod_{i=1}^{N} \varphi_{\mathrm{Ca-He}}(R_i), \tag{26}$$

$$\Psi_{\mathrm{He-He}}(\mathbf{R}) = \prod_{j=1,k=i+1}^{j=N-1,k=N} \varphi_{\mathrm{He-He}}(R_{jk}). \tag{27}$$

$R_i \equiv |\boldsymbol{R}_i|$, $R_{jk} \equiv |\boldsymbol{R}_j - \boldsymbol{R}_k|$ and $\varphi(\cdot) = \exp\{-f(\cdot)\}$, with f the Jastrow functions whose variable and parameters depend on whether we are considering the Ca-He or the He-He interaction:

$$f(R) = \left(\frac{p_5}{R}\right)^5 + \left(\frac{p_3}{R}\right)^3 + \left(\frac{p_2}{R}\right)^2 + p_1 R + p_0 \ln(R). \tag{28}$$

The diffusion equation associated with the Hamiltonian (3), expressed in Cartesian coordinates, is solved by considering Eq. (25) as trial wavefunction. The calculation is performed N_w times, and each of these simulations is called replica or *walker*. The DMC stage relies on the short-time approximation [30] and now the addition of weights to the walkers corrects the variational estimate towards a more realistic expectation value (with the wavefunction fixed). The imaginary time evolves a quantity $\triangle\tau$ on each step. After a large enough number of M steps the distribution function stabilizes on its ground state $\Psi_0\Psi_T$ ("mixed estimator").[31–33]

IV. RESULTS

The masses used were: m(Ca)=40.07878, $m(^4\mathrm{He})$=4.0026, and $m(^3\mathrm{He})$=3.01604 *amu*. For comparisons, the conversion factors 1 K = 0.69503877 cm^{-1} and 1 a_0 = 0.52917726 Å have been employed.

In the variational DVR treatment we have considered 25 points of R in the interval $[2.6, 21.2]$ Å for describing the relevant region of the Ca-He potential[11]. For a total angular momentum $L = 0$, and for boson as well as for singlet fermion systems, up to 31 values, from 0 to 30, of ℓ_1 and ℓ_2 were accounted for, while 101 points of a Gauss-Legendre quadrature in the interval $[-1, 1]$ were used to describe $\cos\gamma = \hat{\boldsymbol{R}}_1 \cdot \hat{\boldsymbol{R}}_2$. In this way, energy convergence to the second decimal figure (cm^{-1}) was achieved. As already mentioned, it is straightforward to obtain probability distributions of R, the Ca-He distance, or $\cos\gamma$[19]. However for R_3, the He-He distance, the calculation of the corresponding distribution is rather expensive and since the DMC and DGF methods produce it in a natural, low time-consuming way, we perform an approximate estimation which rests on the assumption that the distributions of $D(R_1)$, $D(R_2)$ and $D(\cos\gamma)$ are independent. Defining a grid of M equally spaced points in R_3, $\{R_3^{(1)}, R_3^{(2)} = R_3^{(1)} + \Delta, \ldots, R_3^{(M)}\}$, the distribution is obtained by simple binning as

$$D(R_3^{(i)}) \approx \frac{R_L^2}{\Delta(N+1)^2} \sum\sum\sum w_j\, D(R_m)\, D(R_n)\, D(\cos\gamma^{(j)}), \tag{29}$$

where w_j are weights of the Gauss-Legendre angular quadrature, the pre-factor $R_L^2/(N+1)^2$ comes from two Gauss-Chebyshev radial quadratures, and $R_3^{(i)}$ is the nearest value to $R_3 = \sqrt{R_m^2 + R_n^2 - 2R_m R_n \cos\gamma^{(j)}}$ fulfilling the cosine theorem.

With respect to the VMC part we have used the Powell method [34] along a total of $M = 5 \times 10^5$ steps to find the absolute minimum of the trial wavefunction Ψ_T in the space formed by a total of 10 parameters, 5 for each Ca-He and He-He interactions. The number of walkers N_w is ranged between 1000 and 3000, sampled in their propagation through a Langevin procedure, with the variance of E_L as the cost function to be minimized [28, 35]. In the DMC stage of the calculations a similar number of steps have been used; as $50 \leq \triangle\tau \leq 300$ hartree^{-1} a total of $5 \times 10^5 - 1.5 \times 10^8$ hartree^{-1} has been considered, time long enough so as all the quantities were in convergence. The branching scheme for the walkers was that proposed by Blume *et al* [36]. For a fixed N_w we have fitted the energy to a simple straight line $E = m \times \triangle\tau + n$, which tends to n when $\triangle\tau \to 0$. The couples (N_w, n) have been extrapolated, in turn, to the function $n = a + b/N_w$. The parameter we are interested in is a, which is the value of the energy when the number of walkers tends to infinity. The error presented in Table I corresponds to the error associated with the fitting of a. All the shown geometry distributions belong to the calculations with $N_w = 3000$ and $\triangle\tau = 300$ hartree^{-1}.

For the DGF calculations 37 Gaussian functions with centers between 2.1 Å and 21.2 Å with a distance of 0.5 Å between consecutive DGFs were chosen for the He–He distances (R_3), whereas for the two Ca-He distances (R_1 and R_2) and given the difference between the position of the corresponding interparticle potentials (see Fig. 2), the center of the first DGF was taken at 4.8 Å. With this choice a total number of 14254 ϕ_j basis functions in the expansion of Eq. (17) were taken into account. The β parameter of Eq. (22) was taken to be 1.05. A numerical grid of 5000 points between 0.3 Å and 24.9 Å was considered for the numerical integrations.

In Table I we report the results obtained using the three procedures mentioned above for dimers and trimers. For dimers, the system containing boson Helium is more bounded than that with the fermionic partner. This is an expected consequence of the higher mass of ^{4}He as compared with ^{3}He. Both, DMC and DVR methods yield energies in very good agreement, being also very close to exact Numerov calculations (-0.359476 cm^{-1} for Ca-^{3}He, and -0.545039 cm^{-1} for Ca-^{4}He, respectively).

In Fig. 1 we present the DVR distributions of the dimers (multiplied by 10 and referred to its own energy). The maxima of the distributions are located at ≈ 7 Å, a slightly larger distance than the minimum of the PES which is at ≈ 6 Å. The distribution of the fermionic case is more delocalized than in the bosonic scenario, and reflects the difference between the binding energies of the two systems.

	Ca-^{3}He	Ca-^{3}He$_2{}^*$	Ca-^{4}He	Ca-^{4}He$_2$
DMC	-0.362 ± 0.004	-0.778 ± 0.002	-0.5427 ± 0.0006	-1.2242 ± 0.0009
DVR	-0.3575	-0.7631	-0.5450	-1.2174
		-0.3840		-0.8663
DGF		-0.7633		-1.2226
		-0.3835		-0.8916

TABLE I: $L = 0$ energies (cm^{-1}), obtained with the three methods used in this work, for the different species studied. They are measured with respect to the total dissociation limit. For the triatomic complexes, the second row of DVR and DGF results refers to the only excited state obtained for each system.* Singlet fermionic state.

In the case of the trimers we also report in Table I their energies obtained by using the three methods described above. The trimer and dimer energies follow the independent particles model (IPM): E(Ca-^{3,4}He$_2$) $\approx 2\times$ E(Ca-^{3,4}He). All the three methods described above show a good agreement and in the case of the DVR and DGF procedures not only for the ground but also for the single excited state.

For the ground states, in the upper panels of Fig. 2 we plot the Ca-He pair distributions for the trimers Ca-^{4}He$_2$ (left panel) and Ca-^{3}He$_2$ (right panel) calculated by means of the three methods, which essentially produce the same results: in both cases there is a peak at ≈ 7 Å, although in the fermionic case the distribution extends over larger distances than the bosonic one. They are almost identical to the corresponding distributions of the dimers indicating that IPM is fulfilled. The He-He pair distance distributions for bosonic (left panel) and fermionic (right panel) complexes, calculated via the DMC and DGF methods, are shown in the lower panels of Fig. 2. For comparison we also plot approximate DVR distributions obtained by assuming the independence of distributions in the Ca-He distances and cosγ (the latter being shown in Fig. 3) as suggested by the IPM framework. Points were used to stress the approximate character of those DVR distributions. It is worth noticing that "exact" DMC, DGF and approximate DVR results present a remarkable accord and confirms the validity of IPM. However, there is some minor discrepancy between the DGF estimates and the two other methods in the fermionic case, which suggests that the DGF basis should be extended towards longer He-He distances. For bosons, the He-He distance distribution spreads out till ~ 20 Å although presents a clear peak around 5 Å. Provided that the peak of the distribution on Ca-He distances is located near 7 Å, an isosceles arrangement of the trimer with an angle $^4\mathrm{He}-\widehat{\mathrm{Ca}}-^4\mathrm{He}$ of ~ 40 degree, *i.e.* cos$\gamma \sim 0.77$, is found. The distribution of the fermionic species presents a very broad profile which almost extends over the whole accessible spatial region and explores smaller He-He distances than the Ca-He ones as well as linear He-Ca-He arrangements where $R_{\mathrm{He-He}} \sim 2 \times R_{\mathrm{Ca-He}}$. It advances a much more isotropic distribution in cosγ than in the bosonic scenario.

In Fig. 3 we plot angular distributions in terms of cosγ for $^4\mathrm{He}-\widehat{\mathrm{Ca}}-^4\mathrm{He}$ (upper panel) and $^3\mathrm{He}-\widehat{\mathrm{Ca}}-^3\mathrm{He}$ (lower panel) obtained through DVR and DMC methods: they again produce very similar results. According to the previous discussion on He-He distances, boson distribution exhibits a clear peak around cos$\gamma \sim 0.77$, that is, with the helium atoms closer each to the other than both of them are to the calcium atom, although there is a non-negligible probability of collinear He-Ca-He arrangements (cos$\gamma \sim -1$). The fermionic case, although showing a slight preference for the helium atoms to be close each to the other, presents an almost isotropic distribution. In the same figure DVR distributions for the existing first excited state of each species is also depicted: they show a marked population increase around collinear configurations and present a clear nodal pattern. Since the distributions on the $R_{\mathrm{Ca-He}}$ distance are

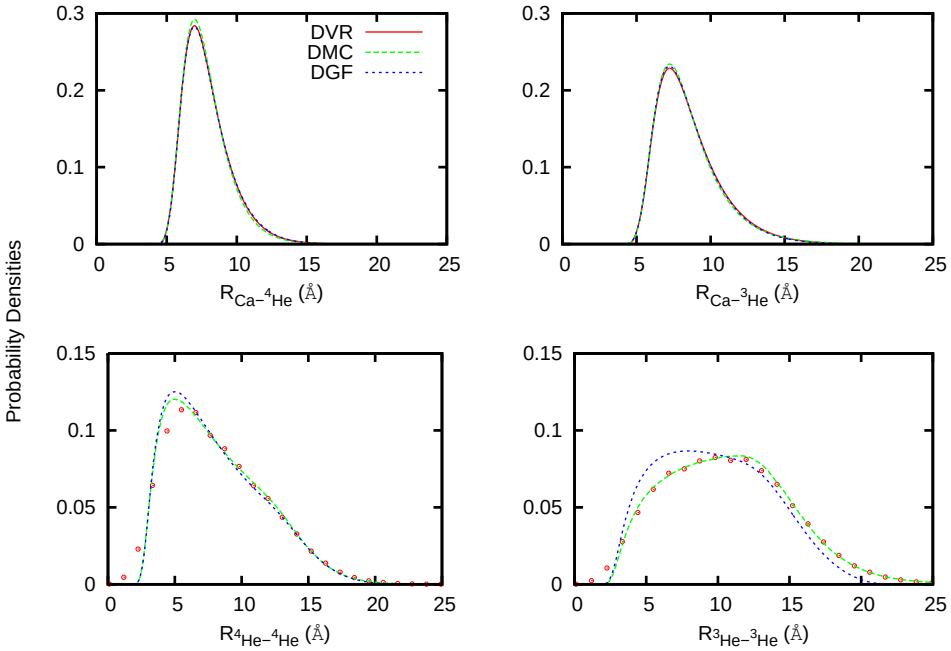

FIG. 2: Comparison of the radial distributions of the Ca-He and He-He distances for the ground states of the two Ca-^{n}He$_2$ complexes obtained using the three different computational methods of the present work. Left panels, bosonic system; right panels, fermionic (singlet) system. Red points in the He-He distance distributions correspond to DVR estimations assuming the independence of probability densities in Ca-He distance and cosγ, see text.

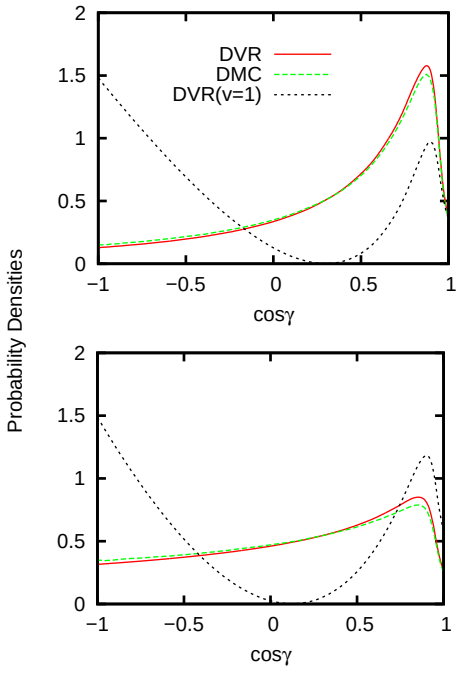

FIG. 3: Angular distributions for Ca-^{n}He$_2$ complexes obtained using the present DVR and DMC procedures. Bosonic/fermionic systems are depicted in the upper/lower panels. The corresponding distributions of the $v = 1$ excited state, obtained through DVR, are also shown.

almost the same than that corresponding to the ground state shown in the upper panels of Fig. 2, see below, one may conclude that they are almost pure excited bending states of the boson or fermion trimers. In this regard, we

should mention the numerical difficulties that the DGF method may present when the system explores quasi-linear geometries. The triangle requirement in Eq. (23) suffices in this case to properly describe both the energy values of excited states and the pair distributions (see below), in good accord with DVR results.

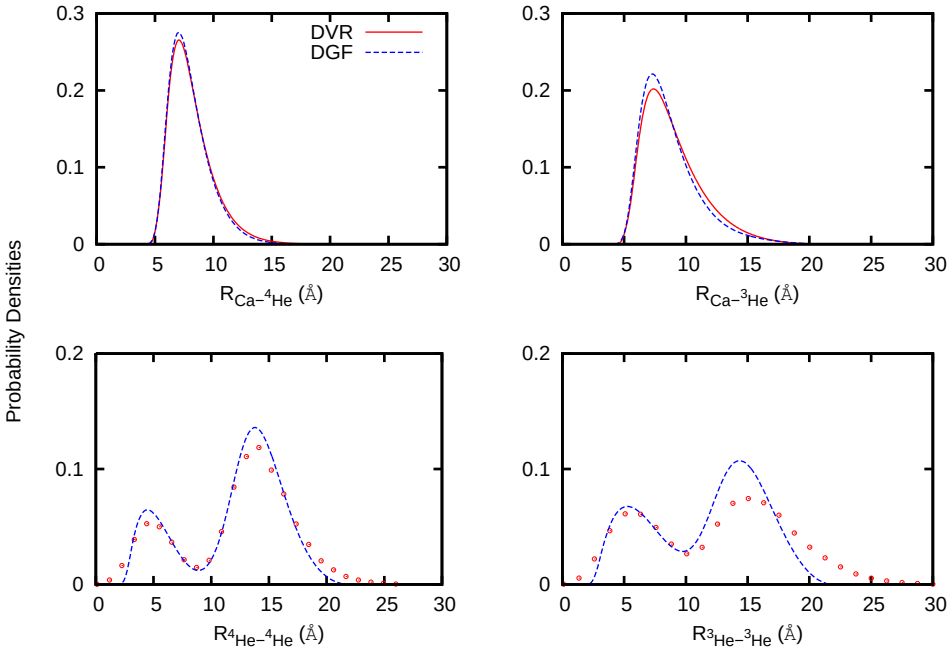

FIG. 4: Distributions of the Ca-He and He-He distances for the excited states of the two Ca-^{n}He$_2$ complexes obtained through DVR and DGF procedures. Left panels, bosonic system; right panels, fermionic (singlet) system. We remark that DVR distributions (with points) of the He-He distance are approximate.

Similarly to Fig. 2, but for excited states, we show at Fig. 4 distributions of Ca-He distances (upper panels) and He-He ones (lower panels) for boson (left panels) and fermion (right panels) systems. Since excited states are unaccessible in the DMC framework, they where calculated through DVR and DGF methodologies. Both distributions of $R_{\mathrm{Ca-He}}$ are essentially the same and differ very little indeed from those corresponding to the ground level (see Fig. 2). Regarding distributions of the He-He distance, we stress that DVR ones are only approximate and are shown by points. In spite of some differences that can be observed, both methods predict the same qualitative features. In particular, the nodal structure obtained in terms of cosγ is well reproduced along the corresponding inter-particle distance. Being cautious again about DVR approximate results, the discrepancies of the DVR/DGF distributions could be attributed to a reduced extension of Gaussian functions accounted for in DGF as it was mentioned above.

V. CONCLUDING REMARKS

In the present work we have endeavored to analyze in some detail the special properties of fairly small clusters of weakly interacting atomic partners: Ca-^{3,4}He$_2$. Such a simple species may provide a useful paradigm for illustrating the general structural features of even larger clusters containing several He atoms. Three very different computational approaches (a discrete variable representation, a distributed Gaussian functions approach and a Variational/Diffusion Monte Carlo technique) have been employed for obtaining relative binding energies and spatial distributions.

The use of a very realistic atom-atom potential for the Ca-He dimer[11] produces only two very weakly bound states in bosonic as well as in singlet fermionic clusters, a very different result from that reported by the calculations of Ref. [15], where an entirely different empirical potential describing the Ca-He interaction[9] has been used. For each species considered the excited state is close to the ground state and not very different from the latter in terms of spatial extension: it chiefly describes a bending excitation of the cluster. Furthermore, the fermionic states are found to be even more weakly bound and also more spatially extended than the bosonic states. For the two species studied, we have shown the fulfillment of the independent particle model.

Regarding ground levels, the radial distributions within the clusters (e.g. see the data in Fig. 2) additionally indicate that the two boson He atoms are closer to each other than both of them are to the calcium "doping" partner:

by extrapolating this feature to larger aggregates (with a much greater network of He-He interactions) one could therefore argue that the calcium atom will eventually locate itself outside the formed cluster of He components, thus confirming the possible formation of a structure where the atomic dopant sits on a "dimple" outside the bosonic droplet. This feature is no longer envisaged for the much more floppy fermionic aggregates as suggested by the data in the right-side panels of Fig. 2, and the Ca atom could become solvated by the ^{3}He environment. This finding is in accord with calculations in the frame of density functional theory[7] which conclude, using a similar Ca-He(^1X) interaction to that used here, that the impurity resides in a deep dimple at the surface of ^{4}He nanodroplets, while it goes to the center of ^{3}He drops. Addressing this point, excitation spectra of alkaline earth atoms attached to helium nanodroplets have been recorded using laser-induced fluorescence spectroscopy[37–39], and more recently through a variety of spectroscopic techniques[40]. In particular, it has been established that Ca atoms reside on the surface of superfluid boson helium nanodroplets[38].

The angular distributions reported by Fig. 3 further suggest an isosceles configuration as the dominant structure for the ground state of the bosonic cluster with a marked spatial delocalization of the He partner atoms attached to the calcium dopant. In the fermion scenario, the structure is much more diffused in such a way that extreme quasi-collinear He-Ca-He and Ca-He-He arrangements are being explored.

In conclusion, we have shown in the present work that it is indeed possible, albeit requiring the use of reliable numerical methods, to gain consistent information on the structures of small, weakly interacting clusters and that such information can help us a great deal to better predict how such systems could spatially grow when one increases the number of He partners in a cluster. In order to make a significant test of the sensivity of the results to the particular choice of the PES, a similar study to the presented here, maintaining the He-He interaction[16] but replacing the Ca-He potential[11] by the stronger interaction[9] as recently used in Ref. [15], is now in progress.

Acknowledgments

The authors thank to Centros de Cálculo IFF-CSIC, CTI-CSIC, and CESGA for allocation of computer time. This work has been partially supported by MICINN, Grants Nos. FIS2010-18132 and FIS2011-29596-C02-01. RRC and DLD acknowledge to the CSIC programs JAE-PREDOC, grant No. JAE-Pre-2010-01277, and JAE-DOC, Contract Id. E-28-2009- 0448699, respectively. FAG thanks the financial support of the PRIN project 2009. The aid of COST Action CM1002 (CODECS) is also appreciated.

[1] J. P. Toennies and A. F. Vilesov, Ang. Chem. Int. Ed. **43**, 2622 (2004).
[2] S. Grebenev, J. P. Toennies, and A. F. Vilesov, Science **279**, 2083 (1998).
[3] F. Paesani, A. Viel, F. A. Gianturco, and K. B. Whaley, Phys. Rev. Lett. **90**, 073401 (2003).
[4] K. N. Barnett and K. B. Whaley, Phys. Rev. A **47**, 4082 (1993).
[5] F. Ancilloto, E. Cheng, M. W. Cole, and F. Toigo, Z. Phys. B Cond. Matt. **98**, 323 (1995).
[6] F. Stienkemeier and A. F. Vilesov, J. Chem. Phys. **113**, 10119 (2001).
[7] A. Hernando, R. Mayol, M. Pi, M. Barranco, F. Ancillotto, O. Bünermann, and F. Stienkemeier, J. Phys. Chem. A **111**, 7303 (2007).
[8] O. Bünermann, M. Dvorak, F. Stienkemeier, A. Hernando, R. Mayol, M. Pi, M. Barranco, and F. Ancilloto, Phys. Rev. B **79**, 214511 (2009).
[9] U. Kleinekathöfer, Chem. Phys. Lett. **324**, 403 (2000).
[10] F. Stienkemeier, F. Meier, K. Stark, and H. O. Lutz, Faraday Discuss. **108**, 212 (1997).
[11] C. C. Lovallo and M. Klobukowski, J. Chem. Phys. **120**, 246 (2004).
[12] E. Czuchaj, M. Krośnicki, and H. Stoll, Chem. Phys. **292**, 101 (2003).
[13] H. Partridge, J. R. Stallcop, and E. Levin, J. Chem. Phys. **115**, 6471 (2001).
[14] R. J. Hinde, J. Phys. B **36**, 3119 (2003).
[15] Q. Gou and Y. Li, Phys. Rev. A **88**, 012510 (2012).
[16] R. A. Aziz and M. J. Slaman, J. Chem. Phys. **94**, 8047 (1991).
[17] I. Baccarelli, G. Delgado-Barrio, F. A. Gianturco, T. González-Lezana, S. Miret-Artés, and P. Villarreal, Phys. Chem. Chem. Phys. **2**, 4067 (2000).
[18] G. A. Natanson, G. S. Ezra, G. Delgado-Barrio, and R. S. Berry, J. Chem. Phys. **81**, 3400 (1984).
[19] P. Villarreal, O. Roncero, and G. Delgado-Barrio, J. Chem. Phys. **101**, 2217 (1994).
[20] J. T. Muckerman, Chem. Phys. Lett. **173**, 200 (1990).
[21] T. González-Lezana, S. Miret-Artés, G. Delgado-Barrio, P. Villarreal, J. Rubayo-Soneira, I. Baccarelli, F. Paesani, and F. Gianturco, Comp. Phys. Comm. **45**, 156 (2002).

[22] I. Baccarelli, F. A. Gianturco, T. González-Lezana, G. Delgado-Barrio, S. Miret-Artés, and P. Villarreal, Phys. Rep. **452**, 1 (2007).
[23] T. González-Lezana, J. Rubayo-Soneira, S. Miret-Artés, F. A. Gianturco, G. Delgado-Barrio, and P. Villarreal, Phys. Rev. Lett. **82**, 1648 (1999).
[24] F. A. Gianturco, F. Paesani, I. Baccarelli, G. Delgado-Barrio, T. González-Lezana, S. Miret-Artés, P. Villarreal, G. B. Bendazzoli, and S. Evangelisti, J. Chem. Phys. **114**, 5520 (2001).
[25] I. Baccarelli, F. A. Gianturco, T. González-Lezana, G. Delgado-Barrio, S. Miret-Artés, and P. Villarreal, J. Phys. Chem. A **110**, 5487 (2006).
[26] I. P. Hamilton and J. C. Light, J. Chem. Phys. **84**, 306 (1986).
[27] E. Coccia, E. Bodo, F. Marinetti, F. A. Gianturco, E. Yildrim, M. Yurtsever, and E. Yurtsever, J. Chem. Phys. **126**, 124319 (2007).
[28] E. Bodo, E. Coccia, D. López-Durán, and F. A. Gianturco, Phys. Scr. **76**, C104 (2007).
[29] F. Marinetti, E. Coccia, E. Bodo, F. A. Gianturco, E. Yurtsever, M. Yurtsever, and E. Yildirim, Theor. Chem. Acc. **118**, 53 (2007).
[30] B. L. Hammond, W. A. Lester *Jr.*, and P. J. Reynolds, *Monte Carlo Methods in Ab-Initio Quantum Chemistry*, World Scientific, Singapore, 1994.
[31] F. Paesani, F. A. Gianturco, M. Lewerenz, and J. P. Toennies, J. Chem. Phys. **111**, 6897 (1999).
[32] S. Bovino, E. Coccia, E. Bodo, D. López-Durán, and F. A. Gianturco, J. Chem. Phys. **130**, 224903 (2009).
[33] R. Prosmiti, G. Delgado-Barrio, P. Villarreal, E. Yurtsever, E. Coccia, and F. A. Gianturco, J. Phys. Chem. A **113**, 14718 (2009).
[34] W. Press, B. Flannery, S. Teukolsky, and W. Vetterling, *Numerical Recipes*, Cambridge University Press, Oxford, U. K., 1986.
[35] D. Bresanini, G. Morosi, and M. Mella, J. Chem. Phys. **116**, 5345 (2002).
[36] D. Blume, M. Lewerenz, F. Huisken, and M. Kaloudis, J. Chem. Phys. **105**, 8666 (1996).
[37] J. Reho, U. Merker, M. R. Radcliff, K. K. Lehmann, and G. Scoles, J. Chem. Phys. **112**, 8409 (2000).
[38] F. Stienkemeier, F. Meier, and H. O. Lutz, J. Chem. Phys. **107**, 10816 (1997).
[39] F. Stienkemeier, F. Meier, and H. O. Lutz, Eur. Phys. J. D **9**, 313 (1999).
[40] E. Loginov and M. Drabbels, J. Chem. Phys. **136**, 154302 (2012).